Crystalfield splittings of gadolinium (4f 7) levels in Ctype rare earth oxides

E. AnticFidancev, M. LemaitreBlaise, and P. Caro

Citation: The Journal of Chemical Physics **76**, 2906 (1982); doi: 10.1063/1.443372
View online: http://dx.doi.org/10.1063/1.443372
View Table of Contents: http://scitation.aip.org/content/aip/journal/jcp/76/6?ver=pdfcov
Published by the AIP Publishing

Crystal-field splittings of gadolinium ($4f^7$) levels in C-type rare earth oxides

E. Antic-Fidancev, M. Lemaitre-Blaise, and P. Caro

Laboratoire des Eléments de Transition dans les Solides, E.R. 210 du CNRS, 1 Place A. Briand, 92190 Meudon-Bellevue, France

(Received 19 October 1981; accepted 24 November 1981)

The absorption spectrum of C-Gd_2O_3 was recorded at room temperature up to 40 600 cm^{-1}. 47 Stark levels of the $4f^7$ configuration were obtained. The fluorescence spectra from the $^6P_{7/2}$ level were recorded for Gd^{3+} in Y_2O_3 and Yb_2O_3. The crystal-field splittings are large. Because of the peculiarities of the half-filled shell, the experimental results (32 Stark levels) were fitted with a C_{2v}-type crystal field Hamiltonian restricted to operators of rank 2 and 4, applied on six different basis sets for $J = 3/2$, 5/2, 7/2 (two matrices), and 9/2 (two matrices) limited by a truncation choice depending on free-ion wave vectors and ignoring J mixing. Real crystal field parameters of rank 2 and 4 were obtained for the C_2 site of C-Gd_2O_3 and are in agreement with those previously determined for Eu^{3+}. The fluorescence data yielded a large value (-1700 cm^{-1}) for the B_0^2 parameter of the S_6 site in C-Y_2O_3.

I. INTRODUCTION

Crystal-field parameters for rare earths in the body-centered cubic C-Y_2O_3 were recently determined.[1,2] However, experimental data for gadolinium were not reported, although the $4f^7$ configuration Stark levels were predicted.[2] The present paper presents the $4f^7$ experimental energy levels for C-Gd_2O_3 in powder form up to 40 600 cm^{-1}, together with the determination of some crystal-field parameters. The $^6P_{7/2}$ position and splitting were also determined for Gd^{3+} in C-Y_2O_3 and for Gd^{3+} in C-Yb_2O_3 also in powder form. The theoretical spectral interest of gadolinium lies in the peculiarity of the $4f^7$ configuration. Experimentally, because the $^8S_{7/2}$ ground state level is scarcely split by the crystal field (usually less than 1 cm^{-1}), the excited states can be determined from absorption at room temperatures.

II. CRYSTALLOGRAPHIC BACKGROUND

The crystallography of the C-type structure is well known. It has been the subject of numerous studies through x rays or neutron diffraction. Accurate position parameters were recently determined[3] and used for *a priori* crystal-field parameter calculations.[1] The space group is T_h^7 and the structure is classically related to that of fluorite with one quarter of the anions missing. Alternatively, one can see it as a tridimensional framework of oxygen-centered OLn_4 tetrahedra (Ln = rare earth) linked together by four edges out of six in the fluorite structure. OLn_4 tetrahedral linkages can be used to describe the lamellar structure of the other two rare earth sesquioxides, the hexagonal A type and the monoclinic B type.[4] From the cation point of view there are two sites: 24 Ln^{3+} in the unit cell lie on the (d) site with point symmetry C_2, eight Ln^{3+} are on the (b) site with point symmetry S_6. The C_2 cations are therefore three times more numerous than the S_6 ones. The great difference between the two sites is that the S_6 point symmetry involves an inversion center whereas, of course, the C_2 does not. As a consequence, dipolar–electric transitions will not be allowed for the rare earth in the S_6 site. The two cation sites are cases of coordination six.

Our powder samples were prepared by the standard method of oxalate decomposition in platinum crucibles for 15 h at 1000 °C from 99.99% pure Pechiney source material. The a cubic parameter of the unit cell for C-Gd_2O_3 was 10.812 Å (the ASTM gives 10.813 Å). For the doped samples we get, for 5% Gd–Y_2O_3 $a = 10.6106$ Å [a (Y_2O_3) = 10.604 Å] and, for 5% Gd–Yb_2O_3, $a = 10.4728$ Å [a (Yb_2O_3) = 10.436 Å].

III. EXPERIMENTAL

The absorption spectra were taken at 300 K directly through thin layers of the powdered oxide. The light source was a xenon 150 W Osram HBO lamp giving a continuous spectrum without xenon emission lines in the UV area. The absorptions were recorded on photographic plates with a 3.4 m Jarrell Ash grating spectrograph. Two lines distant of about 0.0508 Å can be separated with the 590 lines/mm grating in the first order. For doped gadolinium samples the fluoresence spectrum was excited with the xenon lamp. It was composed of lines much sharper than the ones in the absorption spectrum. In that case we have used a holographic grating with a resolving power of 300 000, i.e., the possibility of separating two lines 0.0100 Å apart in the first order.

IV. RESULTS

Sequences of energy levels for the $4f^7$ configuration are known for several compounds.[5–9] There is a quite remarkable difference between the previously reported data and those of the oxide. It is obvious from a qualitative comparison of the spectra[10] that the crystal field splittings are much larger for the $^{2S+1}L_J$ levels in the oxide than they are in compounds such as gadolinium doped $LaCl_3$,[5] the gadolinium ethylsulfate,[8] or $Gd(OH)_3$.[6] As a consequence, labeling the sequence of energy levels is somewhat more difficult because of the possibility of levels overlapping through crystal-field effects.

We will discuss first the C-Gd_2O_3 absorption spectrum. The experimental results are collected in Table I.

The ^6P is the first excited multiplet going up the en-

 0021-9606/82/062906-08$02.10

TABLE I. Energy levels of Gd^{3+} in Gd_2O_3 (all values in cm^{-1}).

Nominal state	Experimental energies	Baricenters	Calculated energies[a]
$^6P_{7/2}$	(31 696)[b]		
	31 728		31 728
	31 821		31 814
	31 865	31 832	31 865
	31 913		31 912
$^6P_{5/2}$	(32 291)[b]		
	32 350		32 356
	32 416	32 409	32 414
	32 461		32 454
$^6P_{3/2}$	32 980		32 981
	33 049	33 015	33 045
$^6I_{7/2}$	35 430		35 453
	35 509		35 504
	35 548	35 523	35 509
	35 606		35 526
$^6I_{9/2}$	35 788		35 805
	35 844		35 834
			35 871
	35 879		35 878
	35 902		35 899
$^6I_{17/2}$	35 943		
	35 978		
	36 060		
	36 114		
	36 141		
	36 184		
	36 206		
	36 225		
$^6I_{11/2}$, $^6I_{15/2}$, $^6I_{13/2}$	36 253		
	36 263		
	36 274		
	36 287		
	36 322		
	36 354		
	36 396		
$^6D_{9/2}$	39 042		39 042
	39 113		39 112
	39 194	39 188	39 194
	39 270		39 273
	39 320		39 318
$^6D_{1/2}$	40 061		
$^6D_{7/2}$	40 155		40 167
	40 184		40 192
	40 199	40 194	40 205
	40 238		40 222
$^6D_{3/2}$	40 333	40 393	40 339
	40 454		40 449
$^6D_{5/2}$	40 454		40 442
	40 562	40 539	40 582
	40 602		40 594

[a]See Table II, giving free-ion parameter values in the calculation.
[b]Level probably belonging to the S_6 site.

ergy scale. Although the lines are broad in the 31 700 to 33 000 cm^{-1} range, one can identify easily three groups of four, three, and two lines corresponding to $^6P_{7/2}$, $^6P_{5/2}$, and $^6P_{3/2}$, respectively, and to a single site. Despite their large half-width the Stark lines are well separated due to the large crystal field (Fig. 1). The transitions from $^8S_{7/2}$ to $^6P_{7/2}$ and $^6P_{5/2}$ are dipolar magnetic in nature and much more intense than the transition to $^6P_{3/2}$. Because of the magnetic dipolar character, one would expect to see also transitions for the S_6 site. In fact, there is no clear doubling but some transitions, notably the lower Stark levels for $^6P_{7/2}$ and $^6P_{5/2}$, seem to have a weaker companion slightly under them. As will be argued later, it is possible that the two sites yield comparable splittings and then the signals will be superposed and that may be one of the sources of the broadness of the C-Gd_2O_3 absorption lines compared to the fluorescence ones from the doped oxides of other rare earths.

The ^6I multiplet is next (Fig. 1). The $^6I_{7/2}$ level is well separated from the others and offers no assignment problem. Then, there is a group which should correspond to $^6I_{9/2}$ and $^6I_{17/2}$. From a comparison of the separation between $^6I_{7/2}$ and $^6I_{9/2}$ for several compounds[9] and the oxide, we suppose that the first four Stark lines in that group belong to $^6I_{9/2}$ (this is supported by the calculations below), and the next two lines at 35 943 and 35 978 cm^{-1} to $^6I_{17/2}$. If this is correct, the splitting for $^6I_{17/2}$ will be at least 35 cm^{-1} whereas it is always very small in other compounds [10 cm^{-1} in $Gd(OH)_3$].[6] The line at 35 943 cm^{-1} is the most intense of the group and the broadest one and may be composed of a superposition of several lines. A second group made of $^6I_{11/2}$, $^6I_{15/2}$, and $^6I_{13/2}$ appear to be composed of 13 distinct absorption lines instead of the theoretical 21. The overall splitting is 335 cm^{-1}, to be compared with 199 cm^{-1} in $Gd(OH)_3$.[6]

The first level of the ^6D multiplet (Fig. 1) is $^6D_{9/2}$, here composed of five sharp absorption lines much stronger in intensity than the other transitions to ^6D_J.

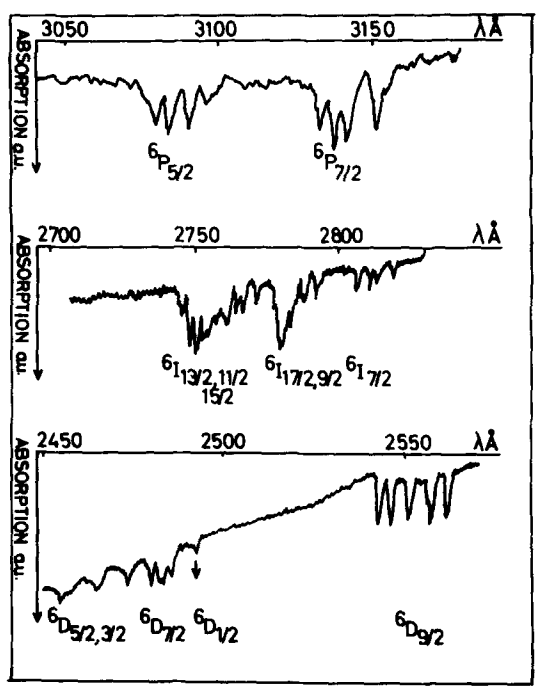

FIG. 1. Absorption spectra at 300 K of Gd^{3+} in C-Gd_2O_3.

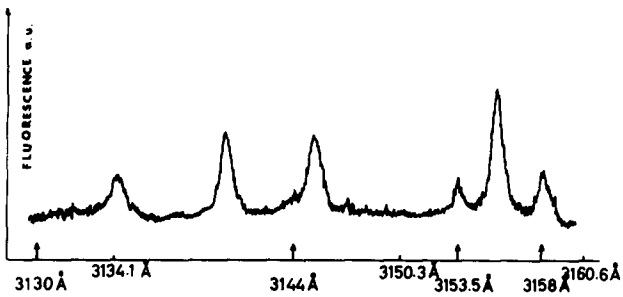

FIG. 2. Fluorescence spectrum of the $^6P_{7/2}$ level of Gd^{3+} in C-Y_2O_3 (300 K).

The overall splitting is large: 278 cm^{-1}, about four times the one in $Gd(OH)_3$. The single weak line at 40 061 cm^{-1} corresponds to the $^6D_{1/2}$ level. Then the $^6D_{7/2}$ level appears as four sharp lines of medium intensity with an overall splitting of 83 cm^{-1}, to be compared with the 13 cm^{-1} recorded for $Gd(OH)_3$. Two weak absorption lines at 40 333 and 40 454 cm^{-1} are attributed to $^6D_{3/2}$. Their separation is 121 cm^{-1}, twice the value for the $^6P_{3/2}$ splitting. The last two observed lines will then belong to $^6D_{5/2}$. It seems that one Stark line is missing for this level. However, a detailed examination of the 40 454 cm^{-1} line shows that this one may be double. If the ground Stark component of $^6D_{5/2}$ is superposed on a Stark component of $^6D_{3/2}$, the two excited $^6D_{5/2}$ Stark levels are at 108 and 148 cm^{-1}. The approximate calculation below yields 143 and 155 cm^{-1} for these excited components, respectively. With this identification the experimental baricenter of $^6D_{5/2}$ should be at 40 539 cm^{-1}, i.e., 345 cm^{-1} above that of $^6D_{7/2}$. The same order of magnitude for this separation is found in other gadolinium salts.[9]

The doped oxides did not give good absorption data due to the low level of doping, but they yielded a fluorescence spectrum from the lower $^6P_{7/2}$ excited level. The lines are sharp (Fig. 2). For the yttrium doped sample two additional lines were clearly recorded which may belong to the energy level scheme of the S_6 site.

The experimental results are collected in Table IV.

V. INTERPRETATION OF THE DATA

A. Building the crystal field matrices

The states of $4f^7$ are divided into two classes depending on their seniority number.[11] There are 119 ^{2S+1}L terms which form 327 $^{2S+1}L_J$ levels, each $(J+\frac{1}{2})$ times degenerate in the absence of a magnetic field. The total number of Kramers doublets is then 1716. States with seniority $v=7$ and 3 belong to class I (for example, ^8S, ^6D, ^6G, and ^6I) and those with seniority $v=5$ and 1 to class II (for example, ^6P, ^6F, and ^6H). Now the configuration is a half-shell and as a consequence there are *no* matrix elements for the spin–orbit and crystal-field interactions among states belonging to the *same* class. Then the observed splittings are only due to spin–orbit and crystal-field interactions between states belonging to different classes, i.e., they are due to off-diagonal matrix elements. There can be spin–orbit operator matrix elements between states of different multiplicities but the crystal-field operators will of course act between states of the same multiplicity.

In those conditions practical computation of crystal-field splittings depends strongly on some sort of truncation choice because it is rather difficult and expensive to build a matrix on the 1716 basis states theoretically needed.

To get a reasonable truncation choice, we neglected J mixing, i.e., we treated the crystal-field problem on a J-value basis. We have seen that this may be a bit of a problem, because we have evidence for the superposition of levels with different J values (but belonging to the same class).

We used the free-ion wave vectors computed by Wybourne[11] as a starting point for the truncation choice.

The $^6P_{7/2}$ free-ion wave vector is as follows [using the symbolism $^{2S+1}_{v}L(U)$ to describe the states, v being the seniority number and U Racah's G_2 representation symbol[12]]:

$$^6P_{7/2} = 0.8514\,|\,^6_5P\rangle - 0.1503\,|\,^8_7S\rangle - 0.4038\,|\,^6_7D\rangle + 0.0713\,|\,^6_5F\rangle + 0.1799\,|\,^4_3D(20)\rangle + 0.1936\,|\,^4_7D(22)\rangle\ .$$

For all states having $J=7/2$, one can build a matrix of size 48×48, using all M_J values, and yielding after diagonalization 24 Kramers doublets. In this matrix the interelectronic repulsion operator—which acts between states of the same class—will be represented by the appropriate combination of Racah's parameters according to the tables of Nielson and Koster. The spin–orbit operator will act between ^6P and the other class states, i.e., ^8S, ^6D, and the two ^4D and also between ^6F and ^6D and $^4_3D(20)$. The crystal-field operators will connect the states of ^6P and ^6F with those of ^6D. Splittings will be obtained as the result of those multiple off-diagonal interactions. ^6P has spin–orbit matrix elements with seven terms in the configuration. We have taken into account here four of those terms. ^6D has in all eight nonzero spin–orbit matrix elements in the configuration, and two are taken into account; ^6F has 10, two also being taken into account. It is clear that ^6D plays here the part of a "splitter state" for ^6P, and indirectly for the ground state $^8S_{7/2}$, the reverse of course being true. However, the Nielson and Koster tables[12] for the U^k operator matrix elements show that there are no matrix elements for k of rank 4 and 6 between ^6P and ^6D. There is only a matrix element for $k=2$. There is a matrix element for ^6D–^6F interaction for $k=2$ and 4 but not for $k=6$. The consequence is that the second order crystal-field operator will play a dominant part in the crystal-field splittings for $^6P_{7/2}$ and $^6D_{7/2}$, the fourth order ones a limited part, and that the sixth order ones are negligible. This was discussed by Jones and Judd.[13]

By giving appropriate values to Racah's parameters, the spin–orbit coupling constant, and crystal-field parameters, the splittings for $^8S_{7/2}$, $^6P_{7/2}$, and $^6D_{7/2}$ can be simulated and compared to experiment. One

TABLE II. Free-ion parameters (all values in cm^{-1}) used for each matrix.

Matrix	$^6P_{7/2}$	$^6P_{5/2}$	$^6P_{3/2}$	$^6I_{7/2}$	$^6I_{9/2}$	$^6D_{9/2}$
E^0	40.507	49.497	49.72	237.31	111.95	64.085
E^1	5743	5743	5743	5550	5743	5743
E^2	26.42	26.42	26.42	26.42	26.42	26.42
E^3	570.6	570.6	580.9	700	570.6	570.6
ζ	1412	1369	1412	1412	1412	1412

should be cautious, however, in that we are using a fairly truncated matrix and that a score of small contributions may sum up into a sizable effect.

The Ref. 11 wave vector for $^6P_{5/2}$, i.e.,

$$^6P_{5/2}:\ 0.8911\left|{}^6_5P\right\rangle - 0.4176\left|{}^6_7D\right\rangle + 0.0638\left|{}^6_5F\right\rangle + 0.1002\left|{}^4_3D(20)\right\rangle + 0.1088\left|{}^4_7D(22)\right\rangle ,$$

gives rise to a 30×30 matrix with basically the same constraints noted for $^6P_{7/2}$.

To reproduce, however correctly, the splittings of both $^6P_{3/2}$ and $^6D_{3/2}$, we had to use not the states which appear in the wave vector for $^6P_{3/2}$ in Ref. 11 but those which appear in the wave vector of $^6D_{3/2}$, i.e.,

$$^6D_{3/2} = 0.9287\left|{}^6_7D\right\rangle + 0.3237\left|{}^6_5P\right\rangle - 0.1262\left|{}^6_5F\right\rangle ,$$

giving rise to a 12×12 matrix and showing that we cannot neglect the contribution of ^6F.

Similarly, a matrix of dimension 40×40 was built to simulate the crystal field splittings of $^6D_{9/2}$ and $^4I_{9/2}$ with, respectively, the $|SLJM_J\rangle$ states of $|^6_7D\rangle$, $|^6_5F\rangle$, $|^6_7G\rangle$, $|^4_5F(20)\rangle$ and $|^6_7I\rangle$, $|^4_5H(21)\rangle$, $|^4_5H(30)\rangle$, $|^6_5H\rangle$. For $^6I_{7/2}$ it was necessary to build a 40×40 matrix also, involving $|^6_7I\rangle$, $|^4_5H(21)\rangle$, $|^4_5H(30)\rangle$, $|^6_5H\rangle$, and $|^6_5P\rangle$.

B. Free ion parameters

The interelectronic repulsion operator has diagonal elements between states of the same class in $4f^7$. As a consequence, Racah's parameters appear on the diagonal of the above matrices. The spin–orbit coupling constant, the other familiar free-ion operator, is of course in the appropriate off-diagonal positions. Numerical values of the parameters should be chosen in order to reproduce correctly the baricenters of the various $^{2S+1}L_J$ levels experimentally observed. The basic set came from the results of a survey of gadolinium spectra in this laboratory [14] They are

$E^1 = 5743\ cm^{-1}$, $E^2 = 26.42\ cm^{-1}$, $E^3 = 570.6\ cm^{-1}$, $\zeta = 1412\ cm^{-1}$,

a set which is not very far from the one used by Schwiesow[15] for six hexagonal crystals [$LnBr_3$, $LnCl_3$, $Ln(OH)_3$, LnF_3]:

$E^1 = 5754.7\ cm^{-1}$, $E^2 = 28.083\ cm^{-1}$, $E^3 = 576.69\ cm^{-1}$, $\zeta = 1477.7\ cm^{-1}$.

He used also interaction parameters and the other magnetic operator parameters. The values of our parameters are distinctly smaller, but the use of a more complete set in Ref. 15 makes a real comparison difficult.

Depending on the particular J values for the matrices, small adjustments were necessary to bring the baricenters of the experimentally observed states in line with those computed. Mostly, E^0 was manipulated and sometimes ζ (for $J=5/2$) or E^3 (for $J=3/2$). The values used for each matrix are given in Table II.

The fluorescence spectra exhibit a definite nephelauxetic effect when going from pure Gd_2O_3 to Y_2O_3 and then Yb_2O_3. To fit the $^6P_{7/2}$ barycenter E^1 was varied from 5743 cm^{-1} for Gd_2O_3 to 5740 cm^{-1} for Gd^{3+} in Y_2O_3 and 5737 cm^{-1} for Gd^{3+} in Yb_2O_3. This certainly translates a change (lowering) in the Slater integrals as the distance to the ligand decreases. However, there are not enough data to determine the change in each of the three Slater integrals (see Table IV). A lowering of any one of the three Slater integrals will diminish the energy difference between the baricenters of $^6P_{7/2}$ and $^8S_{7/2}$ as the difference between the matrix elements is

$$15F_2 + 165F_4 + 3003F_6 .$$

C. Crystal-field parameters

There are two ways to handle the crystal-field parameter problem. One is to ignore approximate values for the parameters and to try to extract them from the data. The other is simply to fill in the known values for Eu^{3+} [1] or other rare earths[2] in the same sort of compounds and compare with experiment. It is interesting to explore the first method because it offers a general procedure to obtain some parameters from the gadolinium spectra easily, and this may be useful when these parameters cannot be obtained from other methods such as electrostatic calculations.

As we have said before, the ^6P levels splittings will be sensitive almost only to crystal-field operators of rank $k=2$. Unless there is no symmetry at all at the site, there will be at the most only two such operators for symmetries such as C_2 and above. The crystal-field parameters are B_0^2 and B_2^2 (the imaginary B_2^2 can always be set to zero by a proper choice of axis). To explore the possible splittings for any system we can take for instance the 48×48 $^6P_{7/2}$ matrix, fill in B_0^2 values covering the probable range in solids, and plot the energy solutions for the four $^6P_{7/2}$ Kramers doublets. This is done Fig. 3. We can see the level order according to their M_J values. The separation between the level with $M_J = \pm\frac{1}{2}$ and the one with $M_J = \pm\frac{3}{2}$

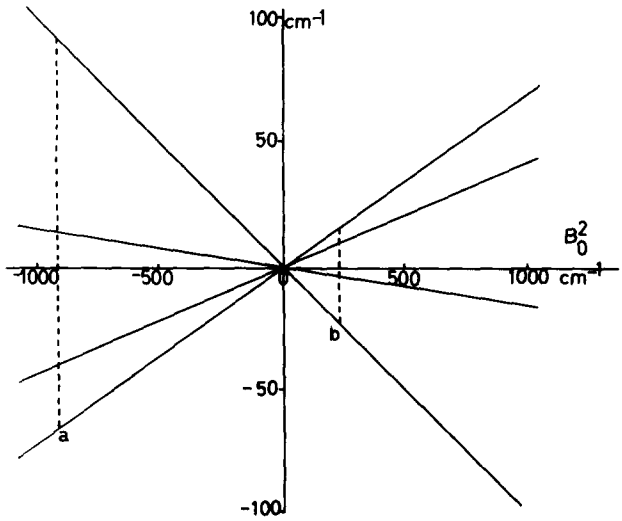

FIG. 3. $^6P_{7/2}$ splitting as a function of the B_0^2 crystal-field parameter: (a) GdOCl, $B_0^2 = -918$ cm^{-1}; (b) Gd^{3+} in $LaBr_3$, $B_0^2 = 230$ cm^{-1}.

is roughly $|B_0^2|/36$, the one between $M_J = \pm\frac{1}{2}$ and $M_J = \pm\frac{5}{2}$ is $|B_0^2|/12$, and between $M_J = \pm\frac{1}{2}$ and $M_J = \pm\frac{7}{2}$ is $|B_0^2|/6$. Then, if we have an axial symmetry, i.e., no B_2^2 parameter, we can find very simply from this diagram an approximate value for the B_0^2 parameter. Take for instance the case of Gd^{3+} in GdOCl, a case of C_{4v} symmetry; the $^6P_{7/2}$ has the following splittings (taking the lowest level as the zero of energy): 0, 25, 76, and 153 cm^{-1}.[16] We immediately see that this unequal separation will fit the left hand side of Fig. 3, i.e., B_0^2 should be negative. More exactly, it corresponds to $B_0^2 = -918$ cm^{-1}, a value which compares well with the experimentally determined one for Eu^{3+} in GdOCl (-907 cm^{-1}).[17] Another example is Gd^{3+} in $LaBr_3$,[6] a case of C_{3v} symmetry. The $^6P_{7/2}$ splittings this time are 0, 19, 32, and 38 cm^{-1}, spacings fitting a positive B_0^2 close to 230 cm^{-1} on the right side of Fig. 3. The experimental value[6] is actually 256 cm^{-1}.

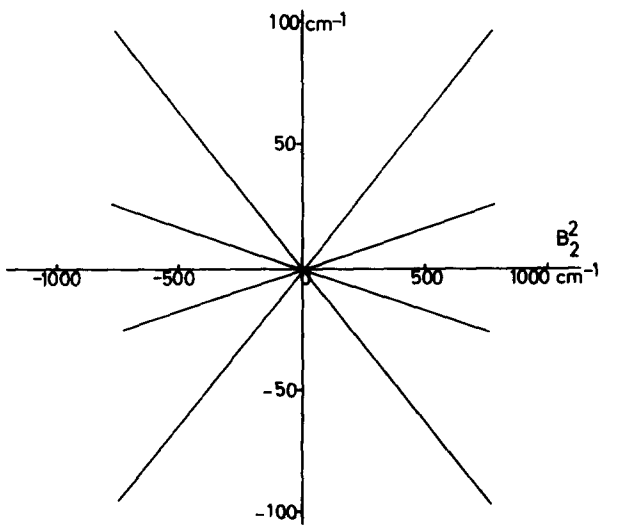

FIG. 4. $^6P_{7/2}$ splitting as a function of the B_2^2 crystal-field parameter.

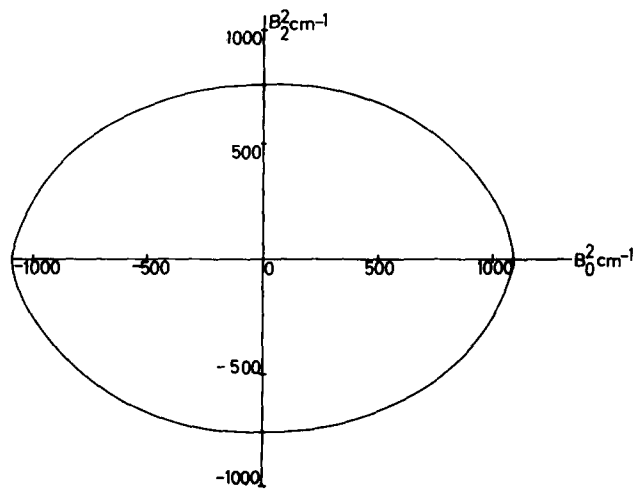

FIG. 5. Locus for the overall splitting of the $^6P_{7/2}$ level in C-Gd_2O_3 as a function of the two crystal-field parameters.

One can remark that the overall splitting of the level is roughly one sixth of the B_0^2 value.

One can draw a similar diagram (Fig. 4) with the B_2^2 parameter alone. In that case, because of the M_J mixing, the levels are more equally spaced and the figure is symmetrical with respect to the sign of B_2^2. There is no experimental example as yet of such a situation. If one should be found, the value of B_2^2 would be roughly four times the overall splitting.

If the symmetry is low, such as in our C_2 case, we have both a B_0^2 and a B_2^2 and the problem is to extract them from the data. To do this we first draw (Fig. 5) a curve which represents the pair of B_0^2-B_2^2 values which will preserve the overall splitting. The curve is drawn for the actual overall splitting of $^6P_{7/2}$ in C-Gd_2O_3, i.e., 185 cm^{-1}. This locus is actually an ellipse. If we plot (Fig. 6) the positions of the two intermediate levels as

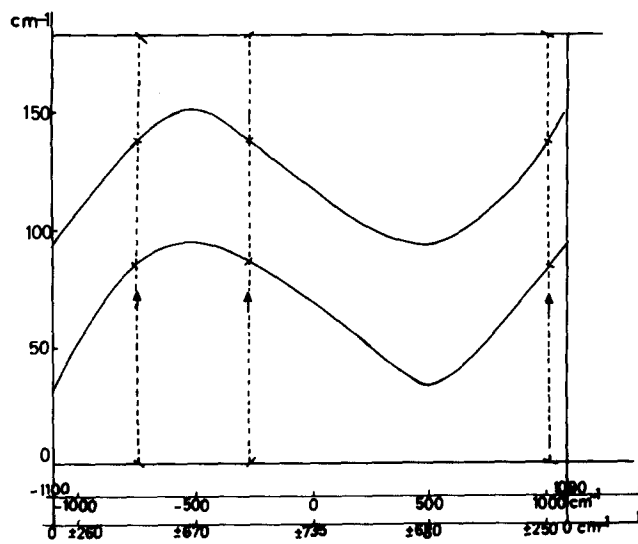

FIG. 6. Evolution of the energies of the two intermediate Stark levels of $^6P_{7/2}$ when the overall splitting is kept constant according to the Fig. 5 locus. Arrows indicate the positions for the three solutions to the experimentally observed levels.

TABLE III. Crystal-field parameters for Gd^{3+} in C-Gd_2O_3 (real parameters for the C_2 site).

Parameter	Gd^{3+}, this study (cm^{-1})	Eu^{3+} in Y_2O_3 Expt., Ref. 1
B_0^2	-266 ± 35	-196 ± 7
B_2^2	-720 ± 15	-695 ± 3
B_0^4	-767 ± 71	-1264 ± 9
B_2^4	-1615 ± 35	-1519 ± 9
B_4^4	932 ± 38	1092 ± 7

we run around the ellipse, we can see that for the particular experimental values we have (0, 93, 137, and 185 cm^{-1}), we will get three solutions for the pair B_0^2–B_2^2. They are, from left to right,

$B_0^2 = -749$ and $B_2^2 = \pm 523$,

$B_0^2 = -266$ and $B_2^2 = \pm 720$,

$B_0^2 = 1012$ and $B_2^2 = \pm 202$ (all in cm^{-1}) .

These sets are rather different, and in a general case they are equally valid on the basis of a knowledge of the energies alone.

In the present case we can immediately decide that the good one is the second set because the experimental results for Eu^{3+} in Y_2O_3 give[1] $B_0^2 = -196$ cm^{-1} and $B_2^2 = -695$ cm^{-1} (the sign is known from PCEM calculations), values astonishingly close to the ones derived here.

This method is general and may be used to obtain probable sets of second rank crystal-field parameters from a knowledge of the $^6P_{7/2}$ Gd^{3+} (or Eu^{2+}) splitting in any compound. If there is ambiguity, one should try to remove it by applying the different sets to results from other probes such as Eu^{3+} or Nd^{3+}, but one of them *is* the good one.

The splittings of $^6P_{3/2}$ and $^6D_{3/2}$ depend only on the B_q^2 parameters, those of $^6P_{5/2}$ and $^6P_{7/2}$ depend to a large extent, as shown, only on them, but $^6P_{5/2}$ is slightly more dependent on B_q^4.

The other levels $^6D_{7/2}$, $^6D_{9/2}$, $^6I_{7/2}$, and $^6I_{9/2}$ depend on both sets of B_q^2 and B_q^4 parameters almost equally; however, $^6D_{5/2}$ is much more sensitive to the fourth order parameters than to the second order ones.

The sixth order parameters have a very small influence on the splittings of those levels and can be neglected.

The second and fourth rank real crystal-field parameters obtained from the adjustment of computed to experimental levels for the C_2 site C-Gd_2O_3 (Table I) are given in Table III. The real fourth order parameters determined for Eu^{3+} in Y_2O_3[1] were used as starting point.

D. Doped samples

For the doped samples the $^6P_{7/2}$ level baricenter is lowered as we go from Gd to Y and to Yb, i.e., when the ionic radius of the cation in the host matrix decreases. In the meantime the splitting of the level increases. This is like applying a "pressure" to the gadolinium ion as the lattice parameter diminishes.

The B_0^2 and B_2^2 parameters were obtained by the same method previously used and the results are in Table IV.

The Auzel *strength parameter*[18] for the crystal field is given in the table and shows that the field increases as the ionic radius of the host cation decreases.

In Ref. 2 values of -209 cm^{-1} for B_0^2 and -728 cm^{-1} for B_2^2 were predicted for Gd^{3+} in Y_2O_3. They compare well with our experimental result, but they are too small, especially B_2^2. This parameter for our doped samples is larger than any of those listed in Ref. 2 for the whole rare earth series doped in Y_2O_3, for which it does not vary much either; the maximum is -804 cm^{-1} for Ce^{3+} and the minimum is -727 cm^{-1} for Eu^{3+}.

TABLE IV. Splittings of $^6P_{7/2}$ in C-type oxides (cm^{-1}).

	C-Gd_2O_3		Gd^{3+}:C-Y_2O_3		Gd^{3+}:C-Yb_2O_3	
	Expt.	Computed[a]	Expt.	Computed[a]	Expt.	Computed[a]
	(31 696)[b]		(31 664)[b]			
$^6P_{7/2}$ (energies)	31 728	31 729	31 690[b]	31 688	31 659	31 658
			(31 711)[b]			
	31 821	31 815	31 793	31 784	31 763	31 756
	31 865	31 867	31 844	31 843	31 817	31 817
	31 913	31 912	31 906	31 903	31 885	31 882
B_0^2	-266 ± 35		-229 ± 45		-198 ± 33	
B_2^2	-720 ± 15		-848 ± 19		-893 ± 13	
$\sqrt{(B_0^2)^2 + (B_2^2)^2}$, Auzel parameter	766		879		915	

[a]See the text for free-ion parameter values in the computation.
[b]Level belonging to the S_6 site.

TABLE V. Calculated energies and corresponding wave vectors for $^8S_{7/2}$.

Stark component E (cm^{-1})	Eigenvector composition
Site C_2 according to B_q^k, Table III	
0	$+0.1123\,\|^6P_{7/2}, \frac{1}{2}\rangle - 0.3689\,\|^8S_{7/2}, \frac{5}{2}\rangle + 0.6961\,\|^8S_{7/2}, \frac{1}{2}\rangle$ $- 0.5700\,\|^8S_{7/2}, -\frac{3}{2}\rangle + 0.1689\,\|^8S_{7/2}, -\frac{7}{2}\rangle$
0.480	$+0.1008\,\|^6P_{7/2}, -\frac{5}{2}\rangle + 0.4790\,\|^8S_{7/2}, \frac{7}{2}\rangle - 0.5468\,\|^8S_{7/2}, \frac{3}{2}\rangle$ $- 0.2340\,\|^8S_{7/2}, -\frac{1}{2}\rangle + 0.6253\,\|^8S_{7/2}, -\frac{5}{2}\rangle$
0.771	$-0.1219\,\|^6P_{7/2}, \frac{7}{2}\rangle - 0.7566\,\|^8S_{7/2}, \frac{7}{2}\rangle - 0.1942\,\|^8S_{7/2}, \frac{3}{2}\rangle$ $+ 0.3016\,\|^8S_{7/2}, -\frac{1}{2}\rangle + 0.5226\,\|^8S_{7/2}, -\frac{5}{2}\rangle$
1.018	$+0.4177\,\|^8S_{7/2}, \frac{5}{2}\rangle + 0.5868\,\|^8S_{7/2}, \frac{1}{2}\rangle + 0.5585\,\|^8S_{7/2}, -\frac{3}{2}\rangle$ $+ 0.3788\,\|^8S_{7/2}, -\frac{7}{2}\rangle$
Site S_6 with $B_0^2 = -1187$ cm^{-1} and $B_0^4 = -1222$ cm^{-1}	
0	$+0.1592\,\|^6P_{7/2}, \frac{1}{2}\rangle + 0.9870\,\|^8S_{7/2}, \frac{1}{2}\rangle$
0.193	$+0.1592\,\|^6P_{7/2}, -\frac{3}{2}\rangle + 0.9870\,\|^8S_{7/2}, -\frac{3}{2}\rangle$
0.563	$+0.1591\,\|^6P_{7/2}, \frac{5}{2}\rangle + 0.9870\,\|^8S_{7/2}, \frac{5}{2}\rangle$
1.103	$+0.1591\,\|^6P_{7/2}, -\frac{7}{2}\rangle + 0.9871\,\|^8S_{7/2}, -\frac{7}{2}\rangle$

We have evidence here that the matrix has a much larger influence than the change in the nature of the doping rare earth element, as far as the second rank parameters are concerned of course.

If we take the lines on Fig. 2 at 31 664 and 31 711 cm^{-1} as coming from fluorescences of the S_6 site, we deduce by the same argument as above that the B_0^2 parameter should be, for this site, close to -1700 cm^{-1}. This compares well with the predicted value from electrostatic calculations of -1200 cm^{-1} for Eu^{3+} in Y_2O_3.[1] Then the other components for the S_6 site should be at 31 807 cm^{-1} (3144 Å) and 31 948 cm^{-1} (3130 Å). The last line is barely visible because the upper Stark levels are de-excited through nonradiative losses. The baricenter for the C_2 site is at 31 808 cm^{-1}, and the one for the S_6 site will be at 31 782 cm^{-1}. The overall splitting for the S_6 site will be slightly larger than that for the C_2 sites and some of the lines, if broad, indeed may overlap as we suggested in describing the C-Gd_2O_3 spectrum.

VI. THE $^8S_{7/2}$ GROUND STATE SPLITTING

The $J=\frac{7}{2}$ matrix yields also the splitting for the ground $^8S_{7/2}$ state. The results together with the wave vectors are listed in Table V for the two sites.

It is well known[11,19] that calculations of the type we are doing here do not reproduce the splitting of the $^8S_{7/2}$ level as measured using ESR experiments. Reasons for this have been discussed at length in the literature.[11,19] However, for the cases investigated, the crystal-field parameters were small. The computed splitting was practically the reverse of the experimental one. This is different when the parameters are much larger. If we take for instance the case of Gd^{3+} in A-La_2O_3, where the cation site has an axial symmetry (C_{3v}), one obtains, using crystal-field parameters determined for Nd^{3+} in pure A-Nd_2O_3,[20] the following order and energies for the $^8S_{7/2}$ Stark levels: $M_J = \pm\frac{1}{2}$ is ground state, $M_J = \pm\frac{3}{2}$ is 0.15 cm^{-1} above, $M_J = \pm\frac{5}{2}$ is 0.448 cm^{-1} above, and $M_J = \pm\frac{7}{2}$ is 0.877 cm^{-1} above. This is a large overall splitting. The order of the levels is in agreement with experiment (contrary to the famous ethylsulfate case[11,19]) but the computed splitting is much smaller than the experimental one, the zero-field splitting determined by ESR techniques,[21,22] which is 0 ($\pm\frac{1}{2}$), 0.28 ($\pm\frac{3}{2}$), 0.78 ($\pm\frac{5}{2}$), and 1.65 ($\pm\frac{7}{2}$) cm^{-1}.

The splitting of $^8S_{7/2}$ is supposed to be a reflection of the splitting of $^6P_{7/2}$, according to the calculation as we have done it. Experience shows that this is not true, and no mechanism has been found to explain the discrepancy satisfactorily. However, the calculation may be quite sensitive to the truncation effect. This is true in other configurations like for instance the $4f^6$ one.[23] and one may wonder if we are not here confronted with the same issue. If one wants to be complete, the $^8S_{7/2}$ splitting problem should be handled with the full set of levels which have a $J=\frac{7}{2}$ in the configuration. There are 50 such levels, all crossed together with matrix elements of spin–orbit or crystal-field operators. To compare really the splittings of excited levels with ESR experiments for the ground state it may be necessary to use the full 400 by 400 matrix.

ACKNOWLEDGMENTS

The authors thank Dr. C. A. Morrison and Dr. J. B. Gruber for kindly making available a manuscript (Ref. 2) before publication.

[1] M. Faucher and J. Dexpert-Ghys, Phys. Rev. B **24**, 3138 (1981).

[2]N. C. Chang, J. B. Gruber, R. O. Leavitt, and C. A. Morrison, J. Chem. Phys. (to be published).
[3]M. Faucher and J. Pannetier, Acta Crystallogr. Sect. B **36**, 3209 (1980).
[4]P. Caro, J. Less Common Metals **16**, 367 (1968).
[5]G. H. Dieke, *Spectra and Energy Levels of RE Ions in Crystals* (Wiley, New York, 1968).
[6]R. L. Schwiessow and H. M. Crosswhite, J. Opt. Soc. Am. **59**, 592 (1969).
[7]A. M. Piksis, G. H. Dieke, and H. M. Crosswhite, J. Chem. Phys. **47**, 5083 (1967).
[8]L. Leopold, dissertation, The Johns Hopkins University, 1958.
[9]H. H. Caspers, S. A. Miller, H. E. Rast, and J. L. Fry, Phys. Rev. **180**, 329 (1969).
[10]P. Caro, E. Antic, L. Beaury, D. Beaury, J. Derovet, M. Faucher, C. Guttel, O. K. Moune, and P. Porcher, Colloq. CNRS **255**, 71 (1977).
[11]B. G. Wybourne, Phys. Rev. **148**, 317 (1966).
[12]C. W. Nielson and G. F. Koster, *Spectroscopic Coefficients for the p^n, d^m and f^0 Configurations* (MIT, Cambridge, Massachusetts, 1963).
[13]H. D. Jones and B. R. Judd, Phys. Rev. B **2**, 2319 (1970).
[14]J. Derouet (private communication).
[15]R. L. Schwiesow, J. Opt. Soc. Am. **62**, 649 (1972).
[16]J. Hölsa (private communication).
[17]J. Hölsa and P. Porcher, J. Chem. Phys. **75**, 2108 (1981).
[18]F. Auzel, Mater. Res. Bull. **14**, 223 (1979).
[19]H. A. Buckmaster, R. Chatterjee, and Y. H. Ching, Can. J. Phys. **50**, 991 (1972).
[20]P. Caro, J. Derouet, L. Beaury, and E. Soulie, J. Chem. Phys. **70**, 2542 (1979).
[21]D. Vivien, A. Kahn, A. M. Lejus, and J. Livage, Phys. Status Solidi B **73**, 593 (1976).
[22]D. Vivien, A. M. Lejus, and R. Collongues, Nouv. J. Chim. **2**, 569 (1978).
[23]G. Teste De Sagey, G. Garon, P. Porcher, and P. Caro, *The Rare Earth in Modern Science and Technology* (Plenum, New York, to be published), Vol. III.